and we now feel confident that this solution can be adopted.

We have however to finish the tests of the final fibre-relay modules in the laboratory. A burn-in test is being discussed with MPE, to be performed with the 4.5W CW sodium laser at Calar Alto. After these tests have been satisfactorily completed, the detailed design activities for the LGSF can be resumed by the second half of next year, pending approval by the ESO management.

References

Ageorges N., Delplancke F., Hubin N., Redfern M. and Davies R.: "Monitoring of laser guide star and light pollution", *SPIE Proceedings* **3763**, in press, 1999.

Avicola et al.: 'Sodium Layer guide-star Experimental Results', *JOSA A*, Vol.**11**, 825–831, 1994.

Bonaccini, D: 'Laser Guide Star Adaptive Optics Performance Analysis', ESO Technical Report VLT-TRE-ESO-11630-1202, 1996.

Christou, J.C., Bonaccini, D., Ageorges, N. and Marchis, F: 'Myopic Deconvolution of Adaptive Optics Images', *The Messenger* No. **97**, 14, Sept. 1999.

Conan, J.M., Fusco, T., Mugnier, L.M., Kersale, E. and Michau, V: 'Deconvolution of Adaptive Optics Images with imprecise knowledge of the point spread function: results on astronomical objects', in ESO/OSA Topical meeting on Astronomy with Adaptive Optics: Present Results and Future Programs, p. 121, D.Bonaccini ed., 1998.

Davies,R, Hackenberg, W., Eckart, A., Ott, T., Butler, D., and Casper, M: 'The ALFA Laser Guide Star operation and results, accepted for publication in *Experimental Astronomy.*

Delplancke F., Ageorges N., Hubin N., O'Sullivan C.: "LGS light pollution investigation in Calar ALto" Proceedings of the ESO/OSA topical meeting on Astronomy with Adaptive Optics, Present Results and Future Programs – Sonthofen, September 1998.

Di Serego Alighieri, S., Bonaccini, D., Oliva, E., Piotto, G., Ragazzoni, R. and Richichi, A: 'Adaptive Optics for the Telescopio Nazionale Galileo', Technical Report No. 41, Astronomical Observatory of Padua-Asiago, 1995.

Fried, D.L. and Belsher, J.F.: 'Analysis of fundamental limits to artificial guide star adaptive optics system performance for astronomical imaging', *JOSA A*, Vol. **11**, p. 277, 1994.

Le Louarn, M., Foy, R., Hubin, N. and Tallon, M.: 'Laser Guide Star for 3.6 and 8m telescopes: performance and astrophysical implications', *MNRAS* **295**, 756, 1998.

Le Louarn, M, Hubin, N., Foy, R. and Tallon, M: 'Sky coverage and PSF shape with LGS-AO on 8m telescopes', *SPIE Proceedings* Vol. **3353**, 364, 1998.

Milonni, P. W. and Fugate, R.Q.: 'Analysis of measured photon returns from Sodium Guide Stars', in Proceedings of the ESO Workshop on Laser Technology for Laser Guide Star Adaptive Optics Astronomy, N. Hubin ed., p. 77, 1997.

Milonni, P.W., Fugate R.Q. and Telle, J.M.: 'Analysis of Measured Photon Returns from Sodium Beacons', *JOSA A*, Vol. **15**, p. 217–233, 1998.

Murray, J.T., Roberts, W.T., Austin, L. and Bonaccini, D.: 'Fiber Raman laser for sodium guide star', in *SPIE Proc.* Vol. **3353**, p. 330, 1998.

Tyler, G.A.: 'Rapid Evaluation of d0: the effective diameter of a laser guide star adaptive optics system', *JOSA A*, **11**, 325, 1994.

Viard E., Delplancke F., Hubin N. and Ageorges N.: "LGS Na spot elongation and Rayleigh scattering effects on Shack-Hartmann wavefront sensor performances", *SPIE Proceedings* **3762**, in press, 1999.

Viard E., Delplancke F., Hubin N., Ageorges N. and Davies R.: "Rayleigh Scattering and laser spot elongation problems at ALFA", accepted for publication in *Experimental Astronomy*.

E-mail: dbonacci@eso.org

VLT Laser Guide Star Facility Subsystems Design

Part I: Fibre Relay Module

W. HACKENBERG, D. BONACCINI, G. AVILA, ESO

The advantages of the LGSF fibre relay approach are twofold: (1) we avoid the cumbersome optomechanical relay, and (2) transfer a diffraction limited beam. The opto-mechanical relay system would require a sealed tube for the laser beam optical path to avoid turbulence and dust contamination, with air-tight sliding joints at the elevation axis, two servo-controlled steering mirrors to keep the optical alignment and several safety interlocks if the beam has lost alignment. Point (2) is very important, as much effort needs to be spent to ensure a good beam quality. Assuming the LGS is an extended object, the adaptive optics wavefront sensor error is proportional to the area of the LGS divided by its flux. As it is both costly and difficult to increase the laser power, all possible efforts have to be taken to minimise the LGS spot size, i.e. the laser beam quality. Some laser relay systems in other LGS projects are even considering incorporating active or low order adaptive optics in the laser beam relay optical path, to ensure a good outgoing beam quality.

Incidentally, injection of high laser power in a single-mode fibre is very useful in long distance fibre communication systems to save repeaters. In fact, much work has been done and literature is available on the subject (Tsubokawa et al., 1986; Cotter, 1982). However the successful injection of several watts of continuous wave (CW) visible laser power has not been demonstrated for long fibres. As we are concerned with a fibre length of 30 m for the VLT LGSF system, we have been able to achieve this in the laboratory and have also learned a few tricks in the process. A fibre relay (Figure 1) provides a very flexible solution and significantly simplifies the integration. It would also be readily applicable to multiple LGS systems needed for future high-order AO systems on large telescopes.

The potential causes of power losses in the fibre are:

1. Coupling losses from the laser beam to the fibre core. These include Fresnel reflections and laser to waveguide mode mismatches..

2. Extinction losses in the bulk material. In a 30 m long low-loss, pure fused silica fibre, the bulk losses from scattering and absorption are expected to be about 8%.

3. Scattering at the fibre core-cladding interfaces.

4. Mode conversion from low-loss trapped modes to high-loss cladding modes.

5. Stimulated Raman Scattering (SRS).

6. Stimulated Brillouin Scattering (SBS).

7. Four-wave mixing between forward and backward Stokes modes.

Points 1 and 6 are the most important causes of losses in our case.

The basic requirements of our fibre relay system (Fig. 1) are:

(i) stable throughput above 70 % over 30 m for 589-nm CW laser light in the multi-Watt regime

(ii) diffraction limited output for the smallest possible LGS spot size

(iii) polarisation preserving.

The latter allows the output of several fibres to be combined, and to circularly polarise the light for the optical pumping of the mesospheric sodium atoms. In order to achieve these requirements, three fundamental problems have to be solved:

1. Efficient coupling of a free-space laser beam into a small-frame optical fi-

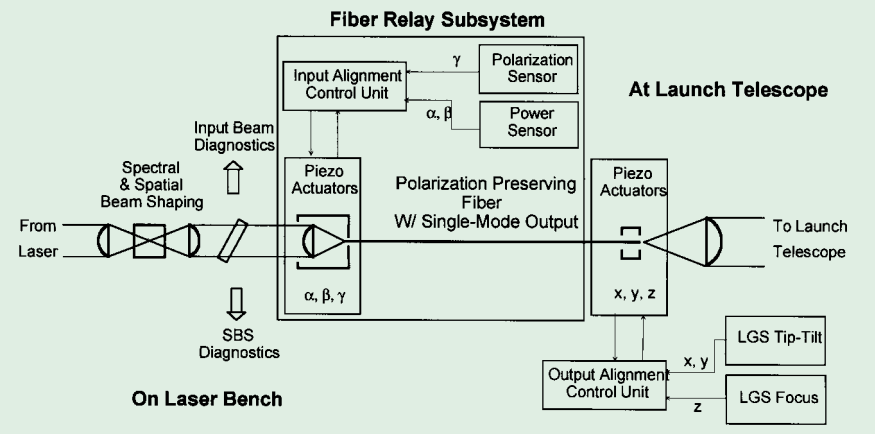

Figure 1: LGSF fibre relay subsystem layout. The fibre input is on the laser optical table, the output is at the launch telescope. The power and polarisation sensors at the fibre end are used to drive the alignment actuators at the fibre input.

bre. This demands an accuracy and long term stability of the order of a fraction of a micron.

2. Handling of high power densities at air-glass interfaces. The power density at the fibre core interface is in the order of several tens of MW/cm^2. This is above the damage threshold of high power anti. reflection coatings (0.5 MW/cm^2). A careful thermal management in the fibre connectors is therefore crucial.

3. Nonlinear effects. At high power levels the scattering processes become stimulated and influence both effective throughput efficiency and spectral purity of the transmitted light.

Three simple measures have been taken to overcome these problems: We have (i) maximised the area of the illuminated air-glass surface, (ii) maximised the effective cross-sectional fibre mode area and (iii) maximised the effective laser line width.

The limits are set by: (i) the numerical aperture of the fibre, (ii) the requirement of having single-mode output, (iii) the finite bandwidth of the mesospheric sodium excitation process.

Design of the Single-Mode Fibre and Input Coupling Unit

The input laser beam at the fibre-waveguide is assumed to be in TEM$_{00}$ mode, i. e. the lowest-order resonator mode. Gaussian beam propagation has to be considered in the design of the coupling optics and their tolerances, so that the mode fields of the input beam and of the optical waveguide optimally match. If we consider a fibre, which is single-mode over its entire length for a given wavelength, the field distribution of the guided fundamental mode can be approximated by a Gaussian. That mode field diameter increases not only with increasing core radius but also with decreasing numerical aperture. The latter is a measure of the light acceptance angle of a fibre. Restricting the waveguide losses due to bending and micro-bending to no more than 1% (minimum bend radius 10 cm) results in a minimum numerical aperture NA = 0.08. For operation as close as possible at the single-mode cut-off wavelength, the maximum fibre core diameter is 5.5 µm for light at 589 nm.

The linear loss coefficient of fibre with a core of pure synthetic fused silica is 0.003 m^{-1} at 589 nm. With antireflection coatings on the fibre ends the theoretical maximum throughput of a 30-m fibre becomes 90%. Since the damage threshold of high-power antireflection coatings is around 500 kWcm^{-2} in the visible, the air-glass surface has to be enlarged at the fibre ends. For this we use a fused silica window, either in optical contact with the fibre or fusion spliced (Fig. 2). To avoid Fabry-Perot effects between the fibre ends, the output surface has to be wedged.

The state of polarisation at the exit of a polarisation-preserving fibre is stable and linear if the input state of polarisation is stable, linear and aligned to the birefringence axis.

For focusing the free-space laser beam onto the fibre we use an aspheric lens, mounted and pre-aligned to the fibre input inside an athermalised housing. We first carried out an analytical optical design, and then verified numerically the coupling efficiency using CODE V. The experiments reported in the last section of this article confirm the design model. Figure 3 shows the dependence of coupling efficiency on decentre between the optical axis and the fibre axis, for various angles of incidence. For optimum coupling efficiency, the incoming laser beam has to be shaped so that the waist diameter of the focal spot produced by the external lens exactly matches the fibre mode field diameter. In our case this is 15 % larger than the nominal core diameter.

Aligning the coupling unit with respect to the incoming beam requires three degrees of freedom. A power and polarisation sensor analysing the fibre output will provide the error signal for a piezo-based servo-loop stabilisation of the optimum injection.

In order to prevent the single-mode contaminating cladding modes (i. e. higher order modes that are not guided by the core), as well as for an optimal heat removal, the fibre connectors have to be fabricated out of glass that matches the fibre core index. A protective and flexible stainless steel sheath is required over the entire length of the fibre.

Critical Fibre Input Power Density

The most important nonlinear loss process in the fibre is stimulated Bril-

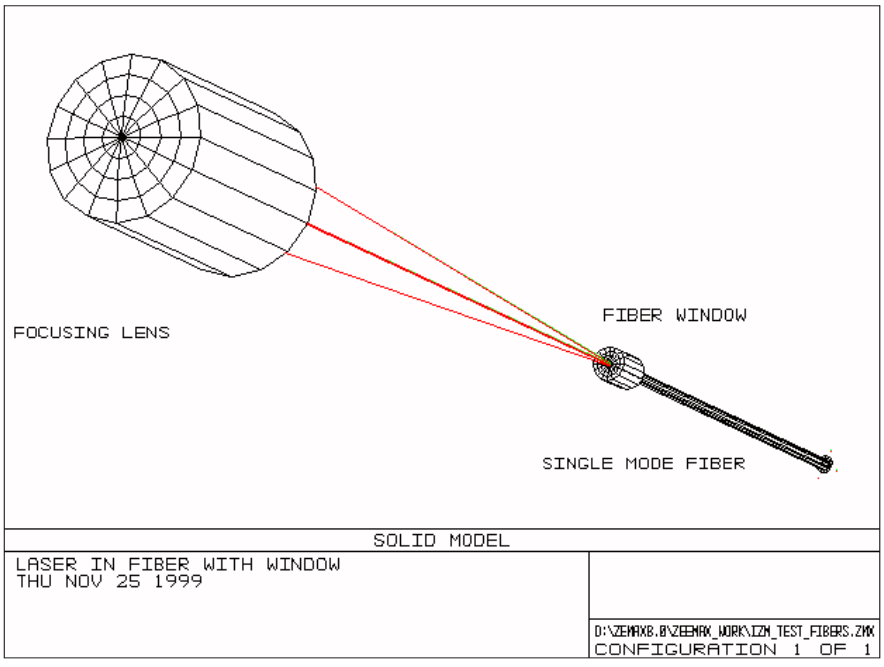

Figure 2: The glass-air interface area of the fibre is enlarged using a window of the same material of the fibre core. The window is either spliced to the fibre, or optically contacted. Both fibre ends have a fibre window.

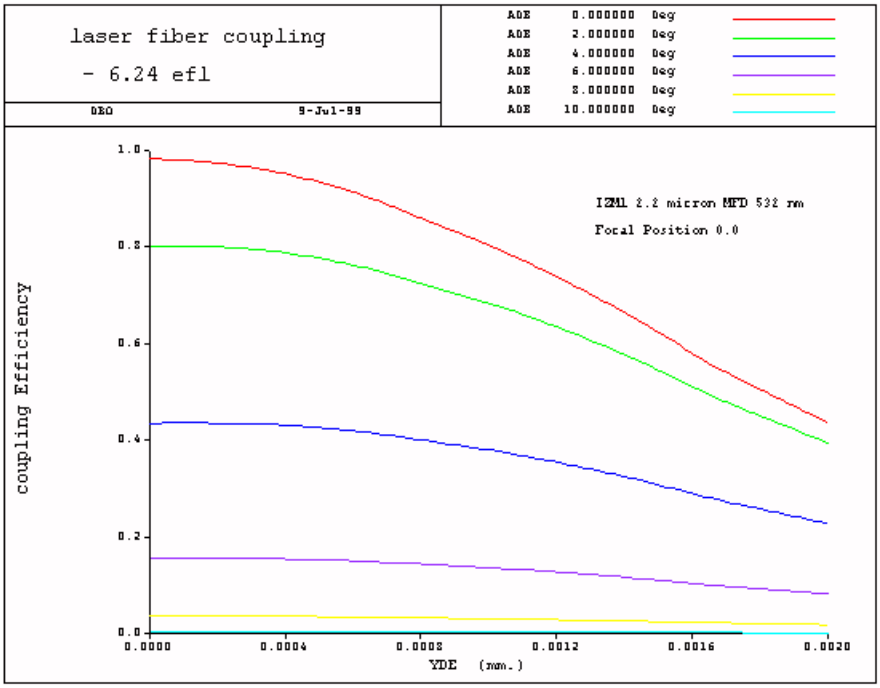

Figure 3: Coupling efficiency for the designed optics. The coupling efficiency is plotted against decentring error between the laser beam and the waveguide axis. Several curves for different beam incident angles are shown.

louin scattering (SBS). This is the scattering of light by sound waves that are created in the fibre by the incident light due to electrostiction[1] in a phonon-photon interaction process. The standing acoustic waves create a regular density grating along the fibre. As a consequence of the selection rules in the waveguide, only scattering in the backward direction occurs in the fibre due to SBS.

[1]The type of piezoelectric effect where the induced material deformation depends on the square of the electrical field amplitude is called electrostiction.

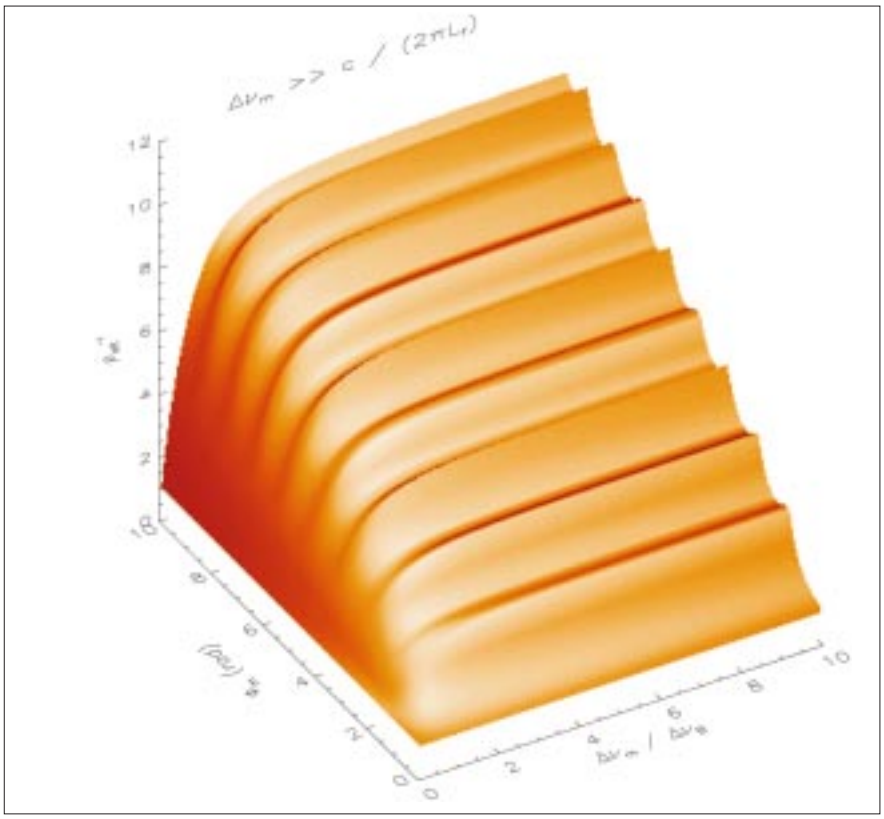

Figure 4: Increase of the SBS threshold pump power, ρ_{eff}^{-1}, under multiline excitation, normalised to the single-mode threshold, as a function of the frequency modulation bandwidth to Brillouin linewidth ratio $\Delta\nu_m / \Delta\nu_B$, and the achievable peak phase shift ϕ_m. It has been assumed that the pump coherence length is much smaller than the fibre length, L_f, and that the frequency modulation is achieved with a single transverse electro-optical modulator.

Energy conservation demands that the amplified backward light (the Stokes wave) is shifted downwards in frequency with respect to the incoming (pump) light, by an amount equal to the acoustic frequency of the material excited. The Stokes line frequency shift is in our case about 30 GHz, and the spectral (or Brillouin) width of the backscatterd light is $\Delta\nu_B$ = 110 MHz FWHM.

The effect of SBS is that a fraction of the light injected in the fibre is sent backwards, shifted in frequency and with a characteristic linewidth of $\Delta\nu_B$. SBS is a non-linear effect and its onset is abrupt, once the pump laser power exceeds a certain threshold. This threshold depends on the fibre material and the frequency distribution of the pump. Solving the differential equations for the Stokes and pump intensities in the steady regime, we obtain a critical pump power[2] of 720 mW. This is for single-frequency, narrow-band sodium light injected into a 30-m single-mode fused silica fibre whose parameters are optimised for minimum power density in the core. In an equivalent polarisation-maintaining fibre the SBS threshold power is reduced by a factor of two due to polarisation scrambling.

As long as the coherence length of the pump light is much smaller than the fibre length, the frequency-dependent SBS gain coefficient is given by the convolution of the pump spectral profile and the SBS gain profile. This is a key point. As it means the critical pump power can be increased, if the effective laser linewidth is broadened, for example by means of phase or frequency modulation of the laser beam.

If we assume a narrow-band single-frequency CW laser source whose effective linewidth is broadened externally by a simple phase modulation scheme (see below), then the pump spectrum will consist of several longitudinal modes equally separated by a frequency $\Delta\nu_m$ corresponding to the modulation bandwidth. The modes of the Stokes wave will be also equidistant, separated by the same distance $\Delta\nu_m$. If again the pump coherence length is much smaller than the characteristic SBS interaction length, i.e. for fibres more than a few metres long, each of the Stokes modes interact with all of the pump modes, and vice versa. Since the interaction strength is determined by the de-tuning from resonance, the interaction bandwidth is limited to the Brillouin linewidth $\Delta\nu_B$. In other words, if $\Delta\nu_m >> \Delta\nu_B$ then the SBS source polarisations generated by different pump modes are not phase matched and do not interfere coherently, as each pump mode generates its own Stoke wave. In this situation and with equal power pump modes, the resulting SBS gain is

[2]Here defined as that input power for which the total SBS power equals 1% of the pump power at the fibre entrance.

reduced by a factor equal to the number of pump modes. This reduction of the SBS gain in case of multimode excitation can be summarised in a factor ρ_{eff}, averaged over all modes and normalised to the SBS gain for a single pump mode with the same total intensity and intrinsic linewidth. In general, ρ_{eff} will also depend on the relative power distribution within the pump modes. For a frequency modulation scheme with a transverse electro-optic light modulator (see below), the relative strength of pump mode *j* is given by the square of the Bessel function of order *j*, evaluated at the peak phase shift ϕ_m which can be achieved with the modulator. The inverse of ρ_{eff} (or the effective increase in the critical input power) is shown in Figure 4 as a function of the externally applied peak phase shift and the frequency modulation bandwidth to Brillouin linewidth ratio. It can be seen that at ϕ_m = 1.5 rad, 2.7 rad, 3.8 rad (etc.) local maxima in ρ_{eff}^{-1} appear. Those extremes correspond to the most equal power distribution within the generated pump modes.

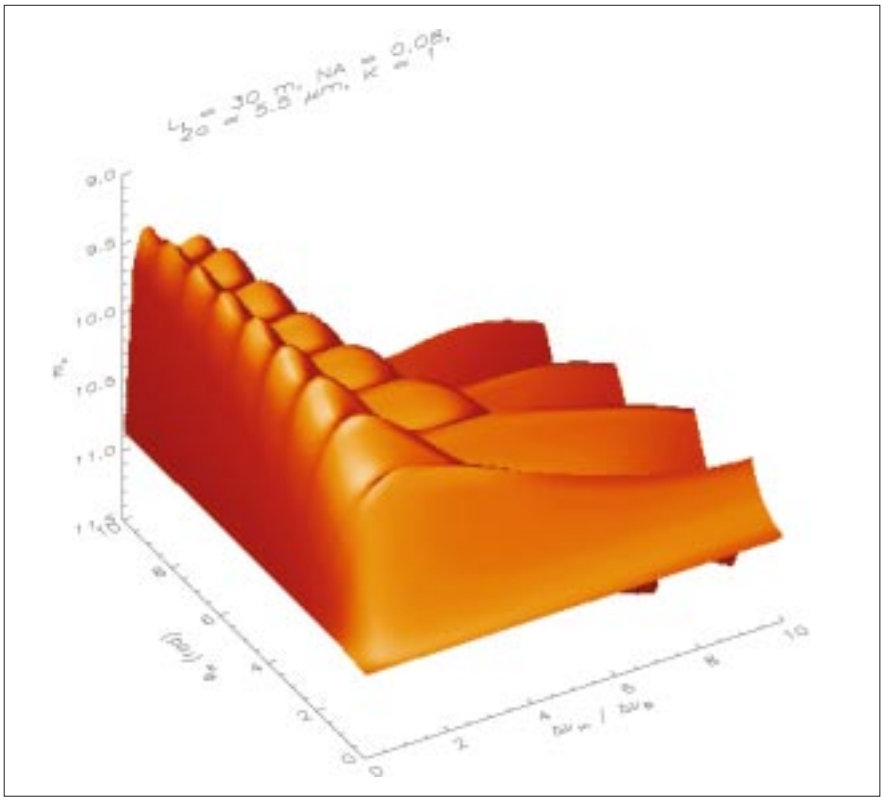

Figure 5: Predicted LGS brightness m_V in case of laser light relay with an optimised single mode, 30-m-long, polarisation-preserving, pure fused silica fibre. The LGS brightness is computed as a function of the frequency modulation bandwidth to Brillouin linewidth ratio, $\Delta\nu_m / \Delta\nu_B$, and peak phase shift ϕ_m, achieved with a single electro-optic modulator. The parameters for the atmosphere are chosen to represent median values. For the transmission of the launching optics 90 % was assumed with the LGS at zenith.

Mesospheric Sodium Excitation Efficiency

The effective backscatter cross section of the mesospheric sodium atoms is given by the convolution of the spectral illumination profile and the sodium absorption profile. We want to maximise it.

With a fixed LGS spot size and increasing layer illumination, saturation of the atoms can be avoided by broadening the effective laser linewidth. Since the width of the Doppler-broadened sodium D_2 absorption profile is about 2 GHz, there is an optimum effective laser linewidth, which optimises the LGS photon return. In Figure 5 the predicted LGS brightness is shown as a function of the phase modulation parameters, in case of a beam relay with an optimised polarisation preserving 30-m-fibre that is single-mode over its entire length.

The throughput of the laser launching optics has been assumed to be 90%. The atmospheric parameters (seeing, transparency, sodium column density, layer height and temperature) assumed for Figure 5 represent median Paranal values, with the telescope pointing the LGS to zenith. As can be seen, the maximum brightness occurs at modulation bandwidth to Brillouin linewidth ratios in the range between 1 and 2. For smaller ratios the lower critical input power limits the brightness, independently of the peak phase shift. For larger bandwidth ratios, the decrease in the overlap integral between the excitation spectral profile and the Doppler-broadened absorption profile limits the LGS magnitude. The brightness gain starts to saturate for optimum peak phase shift values above 2.7 rad. This, together with a minimisation of the electrical power requirements for the laser light modulation, implies an overall optimum peak phase shift of ϕ_m = 3.8 rad. The corresponding optimum modulation to SBS bandwidth ratio is $\Delta\nu_m / \Delta\nu_B$ = 1.0. With these parameters the maximum LGS brightness will be limited to 9.5 equivalent V-band magnitude in case of unpolarised excitation.

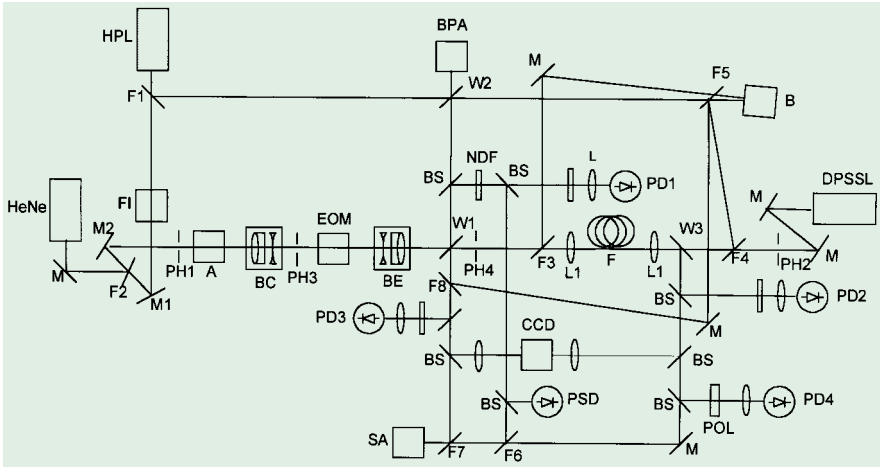

Figure 6: Layout of the laboratory set-up for the results reported in this article. See text for explanation of the acronyms.

Experimental Results

Fibre-transmission experiments have been carried out with the ALFA sodium laser on Calar Alto in 1998. The results of the SBS threshold achieved agree well with theory. In Garching, a prototype injection setup has been built with a 532 nm, 5W CW all solid-state laser. The scheme is shown in Figure 6. HPL is the high power laser. For the laboratory experiment this is a diode-pumped Nd:$YV0_4$ laser (Coherent Verdi) capable of emitting 5.5 W of single-frequency CW power at 532 nm with high beam quality. To suppress any back-reflections into the

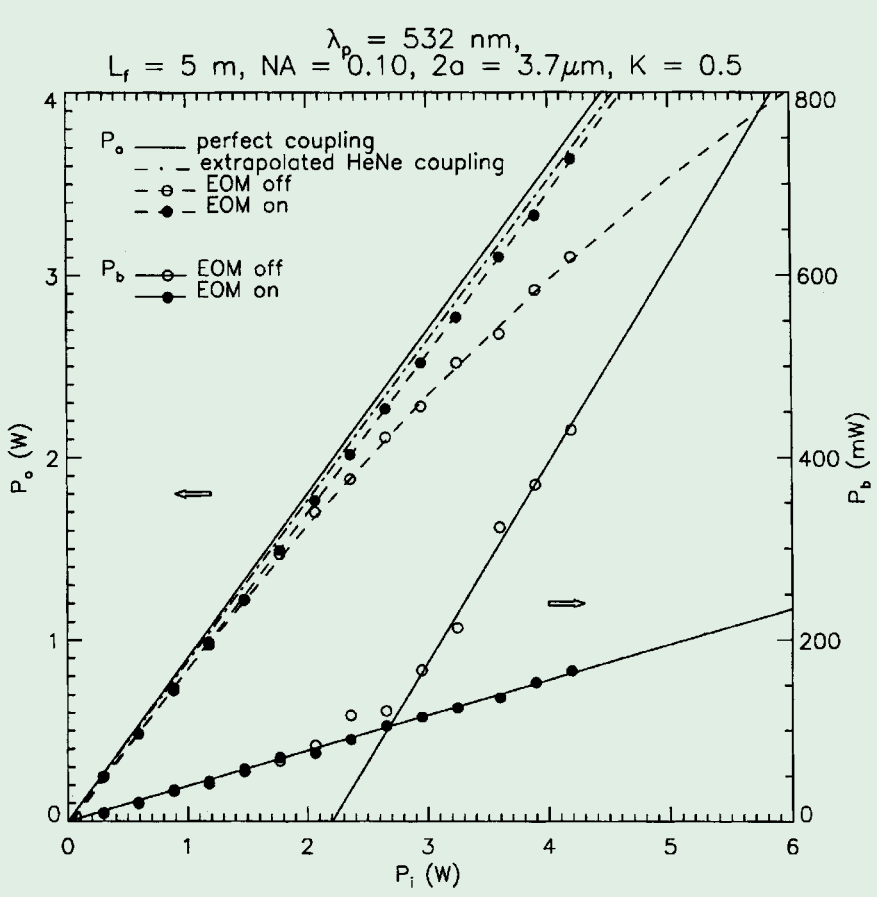

Figure 7: Measured fibre output power P_o and backscattered power P_b as a function of the input power P_i for a 5-m-long pure fused silica non-polarisation preserving single-mode fibre at 532 nm. The cases of unmodulated and frequency modulated input are shown (light modulator EOM on/off). For comparison, the extrapolated low power HeNe-laser transmission and the maximum theoretical throughput is displayed. See text for further details on the setup.

laser head a Faraday Isolator (FI) is installed near the laser output coupler. M1 and M2 are folding mirrors for controlling the four degrees of freedom of the laser beam. PH1-PH4 are pinholes for alignment purposes (see below). For the same reason an attenuator (A) is installed in the beam. Its working principle is based on Fresnel reflection at counter-moving glass plates, which ensures minimum beam position deviation during operation. In combination with the position angle of the exit polariser of FI, any attenuation between 0 dB (without insertion losses) and 27 dB can be selected. BC and BE form the beam shaping optics. These are 2-element 4x beam compressor and expander, respectively. The purpose of these two telescopes is twofold: First, BC reduces the beam size so that the beam can pass through the electro-optical light modulator (EOM) without clipping. The aperture of the electro-optical crystal is minimised in order to relax the electrical power requirements to drive it. Second, by slightly decollimating BC and BE, the waist location and diameter of the beam entering the focusing lens L1 is controlled for optimum launching, i. e. mode matching with the fibre waveguide.

Several diagnostics tools are integrated for on-line analysis of the launched beam, the back-reflected light from the fibre entrance and output. These allow the measurement of the light spectrum (SA), polarisation (POL), power (photodiodes PD 1–4, bolometer B), beam quality (BPA) and jitter as well as waist location and size (beam propagation analyser BPA, position sensitive device PSD). The diagnostics tools are fed with the help of windows (W1–3), beamsplitters (BS) and flipper mirrors (F1–8). Metallic coated neutral density filters (NDF) are used to adjust light levels. All high power lenses and windows including the phase modulator crystal are antireflection coated. The high power mirrors are dielectric coated. To reduce scattering and beam degradation, all high-power surfaces and the elements in the arm of the beam-propagation analyser have a surface quality of better than 60 nm PTV and are polished down to 10^{-5} scratch-dig. The throughput of the high power beam path is 80 %. HeNe and DPSSL are low power lasers for alignment purposes.

To allow the optics in the high-power arm to thermalise and also for safety reasons the coarse-alignment of the high power laser beam is started first with an attenuated beam. Figure 7 summarises the results on the high power transmission of a 5-m-long single-mode test fibre. The conclusion from this first experiment has been that it is possible to achieve an optimum launching and efficient SBS suppression for the test fibre. Moreover, our theoretical calculation and experimental results are in good agreement, which gives us confidence in the reliability of the model of the system. With the current HF amplifier driving the electro-optic light modulator, a maximum peak phase shift of $\phi_m = 2.1$ rad at $\Delta\nu_m = 110$ MHz can be achieved. At 532 nm this corresponds to a SBS gain reduction factor $\rho_{eff} = 0.41$. In Figure 7 the fibre output and backscattered power are shown as a function of the input power on a 5-m-long, non-polarisation-preserving single-mode fibre. Below 2.4 W input power only Fresnel reflection is observed in the backscattered light. This agrees with the calculated critical SBS pump power of 2.5 W. The slight discrepancy between the former values can be explained by the tolerances in the fibre parameters. For input powers higher than 2.5 W and with the laser frequency un-modulated, the SBS back-reflected power increases to 29% of the pump power above the Fresnel reflection. In the spectrum of the back-reflected light the Brillouin-shifted input started to appear at the critical input power. With the modulator switched on, no SBS was observed up to the maximum achievable input power level. This agrees with the calculated decrease of the SBS gain. The modulated throughput at the maximum input level of 4.2 W is 85 %. For comparison the throughput of a low power HeNe-laser is 88 %, measured with an optical setup optimised for the He-Ne laser, which had a mode quality comparable to the Verdi laser. The difference can be explained by the larger beam jitter of the Verdi laser, which should account for nearly 3% coupling loss due to concentricity errors. The maximum theoretical throughput is about 90% including Fresnel reflection at the uncoated fibre end surfaces (8% loss) and extinction (linear loss coefficient 0.005 m^{-1} at 532 nm) but neglecting all other loss sources. The maximum fibre output power was stable during the experiment. A burn-in test with longer fibres is scheduled.

Conclusions

We have demonstrated that a fibre relay module is feasible. The experimental results agree well with the theoretical model. Further work on an optimised, end-face-protected, 30-m-long single-mode fibre is in progress and the first experiments will be carried out in Garching. A burn-in trial on Calar Alto sodium laser is foreseen in the first half of next year.

There appear to be at least two possibilities for further increasing the LGS brightness within a fibre-fed relay system:

1. To combine the polarised output of two fibres at the launch telescope. The brightness limit would increase by 0.7 mag.

2. To separate the two purposes of the fibre relay, namely flexible transportation

of polarised high power light and diffraction-limited output, into two physical fibre sections: a longer multimode section and a shorter mode cleaning section.

The disadvantage of the first solution is the increase in complexity, however we know it is feasible. The advantage of a two-sectioned fibre is that its design would be no longer limited by the critical input power of a single-mode fibre of equivalent length. Instead higher power levels could be considered. For a sodium laser with 10 W output power, whose spectrum is optimised for maximum LGS return flux, a hybrid fibre is under study. Assuming the same launching and atmospheric parameters as for Figure 5, without optical pumping of the sodium atoms via circular polarisation, this laser setup should be able to provide a seeing-limited LGS of brightness V=8 magnitude. This would be sufficient for adaptive optics correction even under poor seeing conditions, pointing at 60 deg Zenith angle.

References

Cotter, D.: 'Suppression of Stimulated Brillouin Scattering during Transmission of High-power narrow-band laser light in monomode fibre', *Electronics Letters*, Vol. **18**, No. 15, p. 638–640, 1982.

Smith, R.G.: 'Optical Power Handling Capacity of Low Loss Optical Fibres Determined by Stimulated Raman and Brillouin Scattering', *Applied Optics*, Vol. **11**, p. 2489, 1992.

Tsubokawa, M, Seikai, S., Nakashima, T., Shibata, N.: 'Suppression of Stimulated Brillouin Scattering in a Single Mode fibre by an Acousto-Optic Modulation', *Electronics Letters,* Vo. **22**, No. 9, p. 473–475, 1986.

E-mail: dbonacci@eso.org

New Pictures from the VLT

Spiral Galaxy Messier 83: This photo shows the central region of a beautiful spiral galaxy, Messier 83, as observed with the FORS1 instrument at VLT ANTU. It is based on a composite of three images, all of which are now available from the ESO Science Data Archive. The three frames were taken in March 1999 through three different filters: B (wavelength 429 nm; Full-Width-Half-Maximum (FWHM) 88 nm; exposure time 10 min; here rendered as blue), R (657 nm; 150 nm; 3 min; green) and I (768 nm; 138 nm; 3 min; red) during a period of 0.8 arcsec average seeing. The field shown measures about 6.8 x 6.8 arcmin and the images were recorded in frames of 2048 x 2048 pixels, each measuring 0.2 arcsec. North is up; East is left.